Theoretical investigation of injection-locked high modulation bandwidth quantum cascade lasers

Meng, Bo; Wang, Qi Jie

2012

Meng, B., & Wang, Q. J. (2012). Theoretical investigation of injection-locked high modulation bandwidth quantum cascade lasers. Optics Express, 20(2), 1450-1464.

https://hdl.handle.net/10356/94708

https://doi.org/10.1364/OE.20.001450

Theoretical investigation of injection-locked high modulation bandwidth quantum cascade lasers

Bo Meng[1] and Qi Jie Wang[1,2,*]

[1]*Division of Microelectronics, School of electrical and electronic engineering, Nanyang Technological University,50 Nanyang Ave., 639798, Singapore*

[2]*Division of Physics and Applied Physics, School of Physical and Mathematical Sciences, Nanyang Technological University, 637371, Singapore*

[*]*qjwang@ntu.edu.sg*

Abstract: In this study, we report for the first time to our knowledge theoretical investigation of modulation responses of injection-locked mid-infrared quantum cascade lasers (QCLs) at wavelengths of 4.6 μm and 9 μm, respectively. It is shown through a three-level rate equations model that the direct intensity modulation of QCLs gives the maximum modulation bandwidths of ~7 GHz at 4.6 μm and ~20 GHz at 9 μm. By applying the injection locking scheme, we find that the modulation bandwidths of up to ~30 GHz and ~70 GHz can be achieved for QCLs at 4.6 μm and 9 μm, respectively, with an injection ratio of 5 dB. The result also shows that an ultrawide modulation bandwidth of more than 200 GHz is possible with a 10 dB injection ratio for QCLs at 9 μm. An important characteristic of injection-locked QCLs is the nonexistence of unstable locking region in the locking map, in contrast to their diode laser counterparts. We attribute this to the ultra-short upper laser state lifetimes of QCLs.

OCIS codes: (060.4080) Modulation; (140.5965) Semiconductor lasers, quantum cascade.

References and links

1. A. Murakami, K. Kawashima, and K. Atsuki, "Cavity resonance shift and bandwidth enhancement in semiconductor lasers with strong light injection," IEEE J. Quantum Electron. **39**(10), 1196–1204 (2003).
2. E. K. Lau, H.-K. Sung, and M. C. Wu, "Frequency response enhancement of optical injection-locked lasers," IEEE J. Quantum Electron. **44**(1), 90–99 (2008).
3. E. K. Lau, X. Zhao, H.-K. Sung, D. Parekh, C. Chang-Hasnain, and M. C. Wu, "Strong optical injection-locked semiconductor lasers demonstrating > 100-GHz resonance frequencies and 80-GHz intrinsic bandwidths," Opt. Express **16**(9), 6609–6618 (2008).
4. N. B. Terry, N. A. Naderi, M. Pochet, A. J. Moscho, L. F. Lester, and V. Kovanis, "Bandwidth enhancement of injection-locked 1.3 μm quantum-dot DFB laser," Electron. Lett. **44**(15), 904–905 (2008).
5. S. H. Lee, D. Parekh, T. Shindo, W. J. Yang, P. Guo, D. Takahashi, N. Nishiyama, C. J. Chang-Hasnain, and S. Arai, "Bandwidth enhancement of injection-locked distributed reflector lasers with wirelike active regions," Opt. Express **18**(16), 16370–16378 (2010).
6. R. Martini, R. Paiella, C. Gmachl, F. Capasso, E. A. Whittaker, H. C. Liu, H. Y. Hwang, D. L. Sivco, J. N. Baillargeon, and A. Y. Cho, "High-speed digital data transmission using mid-infrared quantum cascade lasers," Electron. Lett. **37**(21), 1290–1291 (2001).
7. R. Martini, C. Bethea, F. Capasso, C. Gmachl, R. Paiella, E. A. Whittaker, H. Y. Hwang, D. L. Sivco, J. N. Baillargeon, and A. Y. Cho, "Free-space optical transmission of multimedia satellite data streams using mid-infrared quantum cascade lasers," Electron. Lett. **38**(4), 181–183 (2002).
8. A. Lyakh, C. Pflügl, L. Diehl, Q. J. Wang, F. Capasso, X. J. Wang, J. Y. Fan, T. Tanban-Ek, R. Maulini, A. Tsekoun, R. Go, and C. K. N. Patel, "1.6 W high wall plug efficiency, continuous-wave room temperature quantum cascade laser emitting at 4.6μm," Appl. Phys. Lett. **92**, 111110 (2008).
9. Y. Bai, S. R. Darvish, S. Slivken, W. Zhang, A. Evans, J. Nguyen, and M. Razeghi, "Room temperature continuous wave operation of quantum cascade lasers with watt-level optical power," Appl. Phys. Lett. **92**(10), 101105 (2008).
10. P. Corrigan, R. Martini, E. A. Whittaker, and C. Bethea, "Quantum cascade lasers and the Kruse model in free space optical communication," Opt. Express **17**(6), 4355–4359 (2009).
11. C. Y. L. Cheung, P. S. Spencer, and K. A. Shore, "Modulation bandwidth optimization for unipolar intersubband semiconductor lasers," IEE Proc.: Optoelectron. **144**, 44–47 (1997).

#158118 - $15.00 USD Received 15 Nov 2011; accepted 1 Dec 2011; published 9 Jan 2012

12. C. Y. Cheung and K. A. Shore, "Self-consistent analysis of dc modulation response of unipolar semiconductor lasers," J. Mod. Opt. **45**(6), 1219–1229 (1998).
13. N. Mustafa, L. Pesquera, C. Y. L. Cheung, and K. A. Shore, "Terahertz bandwidth prediction for amplitude modulation response of unipolar intersubband semiconductor lasers," IEEE Photon. Technol. Lett. **11**(5), 527–529 (1999).
14. M. K. Haldar, "A simplified analysis of direct intensity modulation of quantum cascade lasers," IEEE J. Quantum Electron. **41**(11), 1349–1355 (2005).
15. R. Paiella, R. Martini, F. Capasso, C. Gmachl, H. Y. Hwang, D. L. Sivco, J. N. Baillargeon, A. Y. Cho, E. A. Whittaker, and H. C. Liu, "High-frequency modulation without the relaxation oscillation resonance in quantum cascade lasers," Appl. Phys. Lett. **79**(16), 2526–2528 (2001).
16. S. Barbieri, W. Maineult, S. S. Dhillon, C. Sirtori, J. Alton, N. Breuil, H. E. Beere, and D. A. Ritchie, "13 GHz direct modulation of terahertz quantum cascade lasers," Appl. Phys. Lett. **91**(14), 143510 (2007).
17. A. Lyakh, R. Maulini, A. Tsekoun, R. Go, C. Pflügl, L. Diehl, Q. J. Wang, F. Capasso, C. Kumar, and N. Patel, "3 W continuous-wave room temperature single-facet emission from quantum cascade lasers based on nonresonant extraction design approach," Appl. Phys. Lett. **95**(14), 141113 (2009).
18. Q. J. Wang, C. Pflügl, L. Diehl, F. Capasso, T. Edamura, S. Furuta, M. Yamanishi, and H. Kan, "High performance quantum cascade lasers based on three-phonon-resonance design," Appl. Phys. Lett. **94**(1), 011103 (2009).
19. F. Mogensen, H. Olesen, and G. Jacobsen, "Locking conditions and stability properties for a semiconductor laser with external light injection," IEEE J. Quantum Electron. **21**(7), 784–793 (1985).
20. D. Indjin, P. Harrison, R. W. Kelsall, and Z. Ikonić, "Self-consistent scattering theory of transport and output characteristics of quantum cascade lasers," J. Appl. Phys. **91**(11), 9019–9026 (2002).
21. F. Rana and R. J. Ram, "Current noise and photon noise in quantum cascade lasers," Phys. Rev. B **65**(12), 125313 (2002).
22. J. Faist, F. Capasso, D. L. Sivco, C. Sirtori, A. L. Hutchinson, and A. Y. Cho, "Quantum cascade laser," Science **264**(5158), 553–556 (1994).
23. T. Aellen, R. Maulini, R. Terazzi, N. Hoyler, M. Giovannini, J. Faist, S. Blaser, and L. Hvozdara, "Direct measurement of the linewidth enhancement factor by optical heterodyning of an amplitude-modulated quantum cascade laser," Appl. Phys. Lett. **89**(9), 091121 (2006).
24. J. von Staden, T. Gensty, W. Elsäßer, G. Giuliani, and C. Mann, "Measurements of the α factor of a distributed-feedback quantum cascade laser by an optical feedback self-mixing technique," Opt. Lett. **31**(17), 2574–2576 (2006).
25. M. Ishihara, T. Morimoto, S. Furuta, K. Kasahara, N. Akikusa, K. Fujita, and T. Edamura, "Linewidth enhancement factor of quantum cascade lasers with single phonon resonance-continuum depopulation structure on Peltier cooler," Electron. Lett. **45**(23), 1168–1169 (2009).
26. M. S. Taubman, T. L. Myers, B. D. Cannon, and R. M. Williams, "Stabilization, injection and control of quantum cascade lasers, and their application to chemical sensing in the infrared," Spectrochim. Acta A Mol. Biomol. Spectrosc. **60**(14), 3457–3468 (2004).
27. P. Gellie, S. Barbieri, J. F. Lampin, P. Filloux, C. Manquest, C. Sirtori, I. Sagnes, S. P. Khanna, E. H. Linfield, A. G. Davies, H. Beere, and D. Ritchie, "Injection-locking of terahertz quantum cascade lasers up to 35 GHz using RF amplitude modulation," Opt. Express **18**(20), 20799–20816 (2010).
28. C. H. Henry, N. A. Olsson, and N. K. Dutta, "Locking range and stability of injection locked 1.54 μm InGaAsP semiconductor laser," IEEE J. Quantum Electron. **21**(8), 1152–1156 (1985).

1. Introduction

Semiconductor laser sources with high modulation bandwidths are always desirable for high speed data transmission systems. However, the modulation bandwidth of direct modulated semiconductor laser is largely limited by relaxation resonance frequency determined by the interactions of the carriers and photons in the laser cavity. Optical injection locking scheme has been shown theoretically [1] and experimentally [2] as an effective approach to enhance the relaxation resonance frequency of semiconductor lasers, making it a useful method to increase the modulation bandwidth of lasers. With this technique, vertical-cavity surface-emitting lasers (VCSELs) with a 80 GHz intrinsic 3-dB bandwidth [3], quantum-dot (QD) DFB lasers with a 16.3 GHz bandwidth [4], and distributed reflector (DR) lasers with wirelike active regions [5] with a 15 GHz bandwidth have been demonstrated recently.

Quantum cascade lasers (QCLs) are the most promising semiconductor-based mid-infrared and terahertz sources. As they have intrinsic ultrafast intersubband transitions and versatile-designed wavelengths, they are very attractive for high-speed free-space optical (FSO) communication systems [6, 7] (two atmospheric transmission windows are in the regimes (3-5 μm) and (8-14 μm), respectively.) and Light Detection and Ranging (LIDAR)

#158118 - $15.00 USD Received 15 Nov 2011; accepted 1 Dec 2011; published 9 Jan 2012

applications. Recent advancement of high-performance continuous-wave room-temperature operated QCLs [8, 9] has further brought interests of applying QCLs for FSO applications [10]. With direct modulation of 8.1 μm QCLs, enhanced link stability has been demonstrated in FSO communication system in fog weather due to the less Mie scattering at relatively longer wavelengths, showing that QCL is an ideal source for FSO communication in atmospheric conditions with restricted visibility [10]. Earlier theoretical studies show that the modulation bandwidth of QCLs can reach 100 GHz or even Terahertz regimes [11–13]. However, this is misleading as the value of photon lifetime was inaccurately estimated for practical QCLs. Also in [14], the rate equations for QCLs were not correctly established, as the cascade characteristics of QCLs were not properly considered. Direct modulation of QCLs actually leads to a much lower modulation bandwidth ~10 GHz for some mid-infrared QCLs [15] and ~13 GHz for typical terahertz QCLs [16]. Further increase of the modulation bandwidth of QCLs through other approaches is highly desired.

In the paper, we theoretically and systematically investigate the injection-locking of QCLs, for the first time to our knowledge, at emitting wavelengths of 4.6 μm [17] and 9 μm [18] corresponding to the two atmospheric transmission windows, respectively. We first examine the direct intensity modulation characteristics of QCLs, using a three-level rate equations model. The results show that no resonant frequency appears in the frequency modulation response, and the maximum modulation bandwidths of round 7 GHz for QCLs at 4.6 μm and 20 GHz for QCLs at 9 μm are obtained. The theoretical analysis is in good agreement with the experimental observations [15]. In addition, we apply the optical injection locking scheme to increase the frequency modulation bandwidth of QCL. Rate equation analysis shows that the obtained modulation bandwidth of injection locked QCLs is about three times higher than that of the directly modulated QCLs for both lasers at 4.6 μm and 9 μm under a 5 dB injection ratio, with modulation bandwidths up to ~30 GHz and ~70 GHz, respectively. With a 10 dB injection ratio, a modulation bandwidth of over 200 GHz can be achieved with the injection locking scheme. A unique feature of injection locked QCLs is that there is no unstable locking range, as opposed to other semiconductor lasers [19]. We attribute this effect to the ultra-short lifetime of the upper laser state.

2. Theory

2.1 Direct intensity modulation of QCLs

In this study, we use a three-level rate equation model to describe the dynamic behavior of injection-locked QCLs. It is noted that neglecting the carrier number in the lower laser state is invalid in QCLs, especially for room temperature operation, also to accurately describe the dynamic behavior of QCLs, a self-consistent scattering model [20] is required, which however is too complicated for the present study. We denote the instantaneous carrier numbers in the lower and upper laser state by N_2 and N_3, respectively, and the photon number by P. Here the cavity is assumed to have only one longitudinal mode. We noticed that analysis of direct intensity modulation of QCLs with rate equation model has also been investigated in [14]; however, the gain coefficients for carrier rate equations are miscalculated due to the neglect of the cascade characteristics of QCLs. Therefore, the obtained modulation bandwidth in [14] is much larger than that demonstrated in experiments [15]. This conclusion is also supported by the analysis in Ref [21]. The resulted rate equations for QCLs should be:

$$\frac{dN_3}{dt} = J - \frac{N_3}{\tau_3} - \frac{G}{N_p}\left(N_3 - N_2\right)P \tag{1}$$

$$\frac{dN_2}{dt} = \frac{N_3}{\tau_3} + \frac{G}{N_P}\left(N_3 - N_2\right)P - \frac{N_2}{\tau_2} \tag{2}$$

#158118 - $15.00 USD Received 15 Nov 2011; accepted 1 Dec 2011; published 9 Jan 2012

$$\frac{dP}{dt} = G\left(N_3 - N_2\right)P - \frac{P}{\tau_P} \tag{3}$$

where J denotes the current injected into the active region divided by electronic charge e, G is the optical gain coefficient of the entire active region, N_p is the number of stages, τ_2 and τ_3 represent the lifetime of lower and upper laser levels, respectively, and τ_P is the lifetime of photon in the cavity, expressed as $\tau_P = v_g\ (\alpha_w+\alpha_m)$ where α_w, α_m, and v_g are the waveguide loss, mirror loss, and group velocity, respectively. The mirror loss can be calculated using $\alpha_m = -\ln(R_1R_2)/(2L)$, where R_1 and R_2 are the power reflectivity of the facets 1 and 2, respectively. The group velocity v_g is given by $v_g = c/n_{eff}$, where c and n_{eff} are the speed of light in vacuum and modal effective refractive index, respectively. In our analysis, G/N_P instead of G as in [14] is correctly used in Eqs. (1) and (2) to represent the optical gain coefficient of one single active region period in QCLs. Denote $G_0 = G/N_P$, we have $G_0 = \Gamma' v_g\sigma_{32}/V$, where Γ' is the optical mode confinement factor for a single period, and V stands for the volume for a period, given by WLL_P, where W and L are the width and length of the active region, and L_P denotes the period length, respectively. The stimulated emission cross section σ_{32} is,

$$\sigma_{32} = \frac{4\pi e^2 z_{32}^2}{\varepsilon_0 n_{neff}\lambda_0\left(2\gamma_{32}\right)}$$

where e is the electronic charge, z_{32} is the dipole matrix element between the upper and the lower lasing levels, ε_0 is the vacuum dielectric constant, λ_0 is the free-space emission wavelength, and $(2\gamma_{32})$ stands for the full width at half maximum (FWHM) of the optical transition spectrum.

2.1.1 Steady state analysis

We set the time derivatives of Eqs. (1)-(3) to zero, and denote the steady state values of J, N_2, N_3, and P as J_0, N_{20}, N_{30} and P_0, then the steady state rate equations can be expressed as:

$$J_0 - \frac{N_{30}}{\tau_3} - G_0\left(N_{30} - N_{20}\right)P_0 = 0 \tag{4}$$

$$\frac{N_{30}}{\tau_3} + G_0\left(N_{30} - N_{20}\right)P_0 - \frac{N_{20}}{\tau_2} = 0 \tag{5}$$

$$G\left(N_{30} - N_{20}\right)P_0 - \frac{P_0}{\tau_P} = 0 \tag{6}$$

The steady state population of lower lasing level, N_{20} is given as

$$N_{20} = J_0\tau_2 \tag{7}$$

with Eqs. (4) and (5), P_0 can be obtained in the following equation,

$$J_0\left(1-\eta\right) - \frac{N_{30} - N_{20}}{\tau_3} - G_0\left(N_{30} - N_{20}\right)P_0 = 0 \tag{8}$$

where $\eta=\tau_2/\tau_3$. Also, we note that at threshold,

$$\left(N_{30} - N_{20}\right) = \frac{1}{N_p G_0 \tau_p} \tag{9}$$

where J_{th} is the threshold current (s^{-1}), given by $J_{th} = 1/G\tau_3\tau_P\ (1-\eta)$. Substituting Eq. (9) into Eq. (8), one gets the steady state photon number P_0,

#158118 - $15.00 USD Received 15 Nov 2011; accepted 1 Dec 2011; published 9 Jan 2012

$$P_0 = \frac{1}{G_0 \tau_3}\left(\frac{J_0}{J_{th}} - 1\right) \tag{10}$$

with Eqs. (7) and (9), the upper laser level population N_{30} can be written as,

$$N_{30} = \frac{1}{N_P G_0 \tau_P} + J_0 \tau_2 \tag{11}$$

2.1.2 Small-signal modulation analysis

The small-signal analysis is necessary in order to investigate the modulation response of QCLs. Assuming small variations ΔN_2, ΔN_3, ΔP and ΔJ around the steady state values, and substituting $N_2=N_{20}+\Delta N_2$, $N_3=N_{30}+\Delta N_3$, $P=P_0=+\Delta P$ and $J=J_0+\Delta J$ into Eqs. (1) – (3), we get the rate equations for the small deviations as follows:

$$\frac{d\Delta N_3}{dt} = \Delta J - \frac{\Delta N_3}{\tau_3} - G_0\left(\Delta N_3 - \Delta N_2\right)P_0 - G_0\left(N_{30} - N_{20}\right)\Delta P \tag{12}$$

$$\frac{d\Delta N_2}{dt} = \frac{\Delta N_3}{\tau_3} + G_0\left(\Delta N_3 - \Delta N_2\right)P_0 + G_0\left(N_{30} - N_{20}\right)\Delta P - \frac{\Delta N_2}{\tau_2} \tag{13}$$

$$\frac{d\Delta P}{dt} = G\left(\Delta N_3 - \Delta N_2\right)P_0 + G\left(N_{30} - N_{20}\right)\Delta P - \frac{\Delta P}{\tau_P} \tag{14}$$

Taking the Laplace transform of Eqs. (12)–(14), and placing them into a matrix form, we have the following transformed matrix,

$$\begin{bmatrix} s+f_{11} & f_{12} & f_{13} \\ f_{21} & s+f_{22} & f_{23} \\ f_{31} & f_{32} & s+f_{33} \end{bmatrix}\begin{bmatrix} \Delta N_3 \\ \Delta N_2 \\ \Delta P \end{bmatrix} = \begin{bmatrix} \Delta J \\ 0 \\ 0 \end{bmatrix} \tag{15}$$

where the matrix terms are expressed as

$$\begin{aligned} f_{11} &= \frac{1}{\tau_3} + G_0 P_0 & f_{21} &= -\left(\frac{1}{\tau_3} + G_0 P_0\right) & f_{31} &= -GP_0 \\ f_{12} &= -G_0 P_0 & f_{22} &= \frac{1}{\tau_2} + G_0 P_0 & f_{32} &= GP_0 \\ f_{13} &= \frac{1}{\tau_P N_P} & f_{23} &= -\frac{1}{\tau_P N_P} & f_{33} &= 0 \end{aligned} \tag{16}$$

The normalized modulation response is

$$H(s) = \frac{\Delta P}{\Delta J\left(1-\eta\right)\tau_P N_P} = \frac{\frac{s}{A}+1}{Bs^3 + Cs^2 + Ds + 1} \tag{17}$$

Where

$$\begin{aligned} A &= \left(\frac{1}{\eta} - 1\right)\frac{1}{\tau_3} & B &= \frac{\tau_P \tau_2 N_P}{GP_0} \\ C &= B\left(2G_0 P_0 + \frac{1}{\tau_3}\left(1 + \frac{1}{\eta}\right)\right) & D &= B\left(\frac{1}{\tau_2}G_0 P_0 + \frac{1}{\tau_3 \tau_2} + 2GP_0 \frac{1}{\tau_P N_P}\right) \end{aligned} \tag{18}$$

#158118 - $15.00 USD Received 15 Nov 2011; accepted 1 Dec 2011; published 9 Jan 2012

2.2 Injection locking of quantum cascade lasers (QCLs)

2.2.1 Steady state analysis

The injection locking scheme involves two lasers: the slave laser (SL) is optically locked by the master laser (ML) [2]. The differential equation describing electric field inside the slave laser under injection locking was first proposed by Lang and Kobayashi, given as

$$\frac{d}{dt}E_{SL}(t)-\left\{j\omega(N)+\frac{1}{2}\left[N_P G_0\left(N\right)-\frac{1}{\tau_p}\right]\right\}E_{SL}\left(t\right)=f_d E_{ML}\left(t\right) \tag{19}$$

where f_d is the coupling rate between the master laser and the slave laser, approximately expressed as: $f_d = \nu_g(1\text{-}R)/(2LR^{1/2})$ where R stands for the power reflectivity of the injected cavity facet. We denote the electromagnetic fields in the slave laser and the master laser as,

$$E_{SL}\left(t\right)=E_0\left(t\right)e^{j\left(\omega_0 t+\phi_0(t)\right)} \tag{20a}$$

$$E_{ML}\left(t\right)=E_1\left(t\right)e^{j\left(\omega_1 t+\phi_1(t)\right)} \tag{20b}$$

where $E_1(t)$ is taken as a constant, $\phi_0(t)$ and $\phi_1(t)$ are the phases of the two electromagnetic fields, ($\phi_1(t)$ is usually set as zero for computing convenience); ω_0 and ω_1 are the angular frequencies of the slave laser and the master laser, respectively. Substituting Eq. (20) into (19), the differential equation can be split into field magnitude and phase rate equations.

$$\frac{d}{dt}E_0\left(t\right)=\frac{1}{2}N_P G_0\Delta N\left(t\right)E_0\left(t\right)+f_d E_1\cos\phi\left(t\right) \tag{21}$$

$$\frac{d}{dt}\phi\left(t\right)=\frac{1}{2}\alpha N_P G_0\Delta N\left(t\right)-f_d\frac{E_1}{E_0}\sin\phi\left(t\right)-\Delta\omega_{inj} \tag{22}$$

In the above equations, ΔN is the carrier number change due to light injection from the master laser, given by $N\text{-}N_{th}$. Different from rate equations for diode lasers, the carrier number in the above equations is the carrier number difference between the upper and the lower laser levels, i.e. $N = N_3\text{-}N_2$. From Eqs. (12) and (13), and taking into account the carrier number in the lower laser state, the differential equations governing the carrier dynamics are given as,

$$\frac{dN\left(t\right)}{dt}=J-\left(N+N_2\right)\frac{2}{\tau_3}-2E_0^2 G_0 N+\frac{N_2}{\tau_2} \tag{23}$$

$$\frac{dN_2\left(t\right)}{dt}=\left(N+N_2\right)\frac{1}{\tau_3}+E_0^2 G_0 N-\frac{N_2}{\tau_2} \tag{24}$$

where $E_0(t)$, $\phi_0(t)$, $N(t)$, and $N_2(t)$ represent the slave laser's field magnitude, phase, carrier number difference between the transition states, and carrier number in the lower laser state, respectively. The field magnitude $E_0(t)$ has been normalized, so that $|E_0(t)|^2=P(t)$, where $P(t)$ is regarded as the total photon number for a single longitudinal mode inside the cavity. $\phi(t)$ is defined as the phase difference between the master and the slave lasers, i.e. $\phi(t)=\phi_{SL}(t)-\phi_{ML}(t)$, G_0, N_P, α, J, τ_2, and τ_3 are the slave laser's gain coefficient for one stage, the number of period, linewidth enhancement factor, the injection current, the lower laser state lifetime, and the upper laser state lifetime, respectively. While f_d, E_1 and $\Delta\omega_{inj}$ represent the coupling rate, injected electrical field magnitude, and frequency detuning, respectively. The latter is expressed as $\Delta\omega_{inj} = \omega_1\text{-}\omega_0$. For free-running laser, $N = N_{th}$, $N_2 = N_{2th}$, $E = E_{fr}$, with Eq. (24), the carrier number in the lower laser state for free-running slave laser can be obtained,

#158118 - $15.00 USD Received 15 Nov 2011; accepted 1 Dec 2011; published 9 Jan 2012

$$N_{2th} = \left(E_{fr}^2 \gamma_P + \frac{N_{th}}{\tau_3} \right) \frac{\tau_2 \tau_3}{\tau_3 - \tau_2} \tag{25}$$

where we define γ_P as,

$$\gamma_P = G_0 N_{th} \tag{26}$$

Remembering that cavity photon decay rate γ_{P0} is given by GN_{th}, so that $\gamma_P = \gamma_{P0}/N_P$. With Eq. (23) and the expression of γ_P, the threshold current, defined as I/e (where I is current, and e is the electronic charge), and the free-running field magnitude of slave laser are found to be,

$$J_{th} = N_{th} \frac{1}{\tau_3 - \tau_2} \tag{27}$$

$$E_{fr}^2 = \frac{J - N_{th} \dfrac{1}{\tau_3 - \tau_2}}{\gamma_P \dfrac{\tau_3}{\tau_3 - \tau_2}} \tag{28}$$

Under the injection-locking region, the carrier number difference N in the slave laser should decrease, due to the enhanced stimulated mission in the gain medium. The steady state values for E, ΔN, ϕ, and N_2 under injection locking are denoted as E_0, ΔN_0, ϕ_0 and N_{20} respectively. The corresponding expressions of ΔN_0, ϕ_0 and N_{20} are given below,

$$\Delta N_0 = -\frac{2 f_d E_1}{N_p G_0 E_0} \cos \phi_0 \tag{29}$$

$$\phi_0 = \sin^{-1} \left(-\frac{\Delta \omega_{inj} E_0}{f_d E_1 \sqrt{1 + \alpha^2}} \right) - \tan^{-1} \alpha \tag{30}$$

$$N_{20} = \left\lfloor E_0^2 \left(\gamma_P + G_0 \Delta N_0 \right) + \frac{\Delta N_0}{\tau_3} + \frac{N_{th}}{\tau_3} \right\rfloor \frac{\tau_2 \tau_3}{\tau_3 - \tau_2} \tag{31}$$

Applying Eqs. (29)-(31) into Eqs. (23), and setting the time derivative to zero, one gets a cubic equation for the steady state value E_0. Defining two new parameters,

$$T_1 = \frac{2\tau_2 - \tau_3}{\tau_3 - \tau_2} \tag{32}$$

$$T_2 = \frac{2}{\tau_3} + \frac{T_1}{\tau_3} \tag{33}$$

the equation is shown as,

$$E_0^3 \left(2 G_0 N_P \gamma_P + G_0 N_P \gamma_P T_1 \right) - E_0^2 2 G_0 f_d E_1 \cos \phi_0 \left(2 + T_1 \right) - E_0 \left(G_0 J N_P - N_{th} G_0 N_P T_2 \right) - 2 f_d E_1 \cos \phi_0 T_2 = 0 \tag{34}$$

The steady state value of E_0 can be solved by various numerical methods, given that the phase difference ϕ_0 varies approximately from $-\pi/2$ to $\cot^{-1}\alpha$ in the injection locking range, and ΔN_0 should be negative.

#158118 - $15.00 USD Received 15 Nov 2011; accepted 1 Dec 2011; published 9 Jan 2012

2.2.2 Small-signal modulation analysis

Assuming a small variances ΔE, $\Delta\phi$, ΔN and ΔN_2 around the corresponding steady state value, and substituting $E=E_0+\Delta E$, $\phi=\phi_0+\Delta\phi$, $N=N_0+\Delta N$, $N_2=N_{20}+\Delta N_2$ into Eqs. (21) – (24), one gets the rate equations for the small signal modulation:

$$\frac{d}{dt}\Delta E = \frac{1}{2}N_P G_0 \Delta N_0 \Delta E - f_d E_1 \sin\phi_0 \Delta\phi + \frac{1}{2}N_p G_0 E_0 \Delta N \tag{35}$$

$$\frac{d}{dt}\Delta\phi = f_d \frac{E_1}{E_0^2}\sin\phi_0 \Delta E - f_d \frac{E_1}{E_0}\cos\phi_0 \Delta\phi + \frac{\alpha}{2}N_P G_0 \Delta N \tag{36}$$

$$\frac{d}{dt}\Delta N = \Delta J - \left(4E_0\gamma_P + 4E_0 G_0 \Delta N_0\right)\Delta E - \left(\frac{2}{\tau_3} + 2E_0^2 G_0\right)\Delta N + \left(\frac{1}{\tau_2} - \frac{2}{\tau_3}\right)\Delta N_2 \tag{37}$$

$$\frac{d}{dt}\Delta N_2 = \left(2E_0\gamma_P + 2G_0\Delta N_0 E_0\right)\Delta E + \left(\frac{1}{\tau_3} + E_0^2 G_0\right)\Delta N + \left(\frac{1}{\tau_3} - \frac{1}{\tau_2}\right)\Delta N_2 \tag{38}$$

Converting the rate equations into the matrix form and taking Laplace transform, we have the following matrix:

$$\begin{bmatrix} Q_{11}+s & Q_{12} & Q_{13} & Q_{14} \\ Q_{21} & Q_{22}+s & Q_{23} & Q_{24} \\ Q_{31} & Q_{32} & Q_{33}+s & Q_{34} \\ Q_{41} & Q_{42} & Q_{43} & Q_{44}+s \end{bmatrix} \begin{bmatrix} \Delta E \\ \Delta\phi \\ \Delta N \\ \Delta N_2 \end{bmatrix} = \begin{bmatrix} 0 \\ 0 \\ \Delta J \\ 0 \end{bmatrix} \tag{39}$$

In which the matrix elements are

$$\begin{array}{llll} Q_{11} = -\frac{1}{2}G_0\Delta N_0 N_P & Q_{12} = f_d E_1 \sin\phi_0 & Q_{13} = -\frac{1}{2}G_0 E_0 N_P & Q_{14} = 0 \\ Q_{21} = -f_d \frac{E_1}{E_0^2}\sin\phi_0 & Q_{22} = f_d \frac{E_1}{E_0}\cos\phi_0 & Q_{23} = -\frac{\alpha}{2}G_0 N_P & Q_{24} = 0 \\ Q_{31} = 4E_0\gamma_P + 4E_0 G_0 \Delta N_0 & Q_{32} = 0 & Q_{33} = \frac{2}{\tau_3} + 2E_0^2 G_0 & Q_{34} = \frac{2}{\tau_3} - \frac{1}{\tau_2} \\ Q_{41} = -\left(2E_0\gamma_P + 2G_0\Delta N_0 E_0\right) & Q_{42} = 0 & Q_{43} = -\left(\frac{1}{\tau_3} + E_0^2 G_0\right) & Q_{44} = \left(\frac{1}{\tau_2} - \frac{1}{\tau_3}\right) \end{array} \tag{40}$$

The direct modulation frequency response is given by,

$$H(s) = G\frac{s^2 + Es + F}{s^4 + As^3 + Bs^2 + Cs + D} \tag{41}$$

where

#158118 - $15.00 USD Received 15 Nov 2011; accepted 1 Dec 2011; published 9 Jan 2012

$$
\begin{aligned}
A &= Q_{11} + Q_{22} + Q_{33} + Q_{44} \\
B &= Q_{33}Q_{44} + Q_{11}Q_{33} + Q_{11}Q_{44} + Q_{22}Q_{33} + Q_{22}Q_{44} + Q_{11}Q_{22} - Q_{21}Q_{12} - Q_{31}Q_{13} - Q_{34}Q_{43} \\
C &= Q_{11}Q_{33}Q_{44} + Q_{22}Q_{33}Q_{44} + Q_{33}Q_{11}Q_{22} + Q_{44}Q_{11}Q_{22} - \\
&\quad Q_{33}Q_{21}Q_{12} - Q_{44}Q_{21}Q_{12} - Q_{13}Q_{31}Q_{22} - Q_{13}Q_{31}Q_{44} + \\
&\quad Q_{12}Q_{31}Q_{23} + Q_{13}Q_{34}Q_{41} - Q_{22}Q_{43}Q_{34} - Q_{11}Q_{34}Q_{43} \\
D &= Q_{11}Q_{22}Q_{33}Q_{44} - Q_{12}Q_{21}Q_{33}Q_{44} + Q_{12}Q_{21}Q_{43}Q_{34} - Q_{13}Q_{31}Q_{22}Q_{44} + Q_{12}Q_{31}Q_{23}Q_{44} \\
&\quad - Q_{12}Q_{23}Q_{34}Q_{41} + Q_{13}Q_{22}Q_{34}Q_{41} - Q_{11}Q_{22}Q_{34}Q_{43} \\
E &= -\left(Q_{12}Q_{23} - Q_{13}Q_{22} - Q_{13}Q_{44}\right)/Q_{13} \\
F &= -\left(Q_{12}Q_{23}Q_{44} - Q_{13}Q_{22}Q_{44}\right)/Q_{13} \\
G &= -Q_{13}
\end{aligned}
\tag{42}
$$

3. Results and discussions

3.1 Direct modulations

First, we examine the direct modulation bandwidths of QCLs at different wavelengths in the mid-IR regime. Table 1 shows the parameters used in the simulations, of the state-of-the-art mid-infrared QCLs emitting at around 4.6 μm [17] and 9 μm [18], which correspond to the two atmospheric windows in the mid-infrared spectrum range. A simple way to analyze the modulation behavior of QCLs can be done by analyzing the zeros and poles of the normalized frequency response H(s). Tables 2 and 3 list the corresponding zeros and poles for the QCLs at 4.6 μm and 9 μm under different injection currents. Three poles can be obtained from the denominator of the frequency response, which are expressed as p_1, p_2 and p_3 respectively. One zero will be obtained from the numerator. Also shown is the calculated 3-dB bandwidth of the modulation response. We also notice that the phenomena that no resonance frequency appears and the calculated direct modulation bandwidth are in good agreement with the experimental observations [15], if the experimental parameters [15] are used in the calculations.

Table 1. Characteristic parameters of the state-of-the-art QCLs at 4.6 μm [17] and 9 μm [18] for direct modulation

Parameter	Symbol	Value (unit)
Wavelength	Λ	4.6 (μm)/ 9 (μm)
Width	W	11.6 (μm)/12 (μm)
Length	L_p	5 (mm)/ 3 (mm)
Length of period	L	50 (nm)/ 67 (nm)
Modal effective refractive index	n_{eff}	3.27/ 3.27
Waveguide loss	α_W	2.6 (cm^{-1})/ 8.77(cm^{-1})
Mirror loss	α_m	1.34(cm^{-1})/ 2.23 (cm^{-1})
Photon lifetime	τ_p	27.6 (ps)/9.91 (ps)
Upper state lifetime	τ_3	1.77 (ps)/0.66 (ps)
Lower state lifetime	τ_2	0.26 (ps)/ 0.14(ps)
Optical gain coefficient	G	2.93×10^4(s^{-1})/1.2×10^5(s^{-1})
Number of period	N_P	40/40

Table 2. Poles, zeros, and f_{3dB} for QCLs at 4.6 μm

I_0	p_1(GHz)	p_2(GHz)	p_3(GHz)	z(GHz)	f_{3dB}(GHz)
1.5 I_{th}	–2.0	–122.7	–697.5	–552.4	3.4
2 I_{th}	–2.9	–150.0	–759.1	–552.4	5.0
3 I_{th}	–3.9	–190.7	–897.3	–552.4	6.8

#158118 - $15.00 USD Received 15 Nov 2011; accepted 1 Dec 2011; published 9 Jan 2012

4 I_{th}	–4.4	–217.8	–1049.5	–552.4	7.6

Table 3. Poles, zeros, and f_{3dB} for QCLs at 9 μm

I_0	p_1(GHz)	p_2(GHz)	p_3(GHz)	z(GHz)	f_{3dB}(GHz)
1.5 I_{th}	–5.4	–312.7	–1312.5	–907.2	9.4
2 I_{th}	–8.1	–364.5	–1499.1	–907.2	14.0
3 I_{th}	–10.8	–428.8	–1914.4	–907.2	18.6
4 I_{th}	–12.2	–464.7	–2359.4	–907.2	21.0

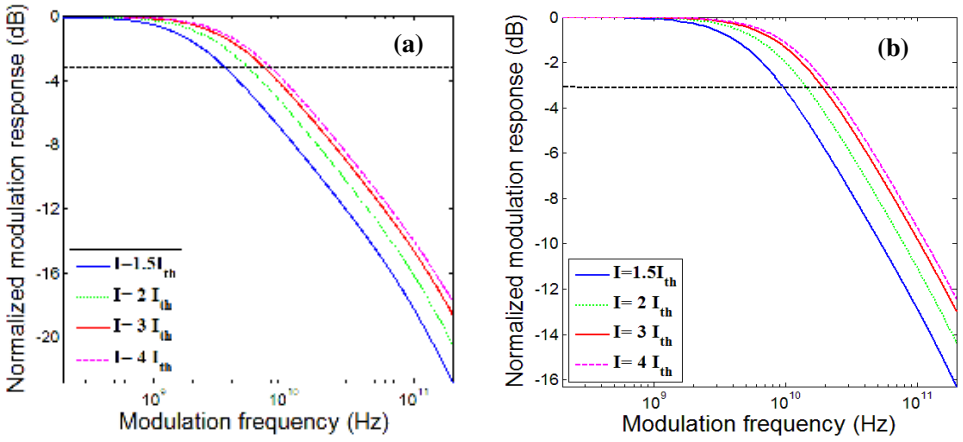

Fig. 1. Normalized modulation response of mid-infrared QCLs. (a) QCLs emitting at 4.6 μm with parameters shown in Table.1 (b) QCLs emitting at 9 μm with parameters shown in Table.1. The 3-dB bandwidth is indicated by the black dashed line.

Figures 1(a) and (b) show the normalized frequency responses of QCLs at 4.6 μm and 9 μm, for $I = 1.5I_{th}$, $2I_{th}$, $3I_{th}$, and $4I_{th}$, respectively, corresponding to the injection currents from just above threshold to roll-over, respectively. Obtaining the poles and zeros of the frequency response, we can transfer it into the following form,

$$H(s) = \frac{\left(\frac{s}{|z_1|}+1\right)}{\left(\frac{s}{|p_1|}+1\right)\left(\frac{s}{|p_2|}+1\right)\left(\frac{s}{|p_3|}+1\right)} \tag{43}$$

This is the normal form of the Bode plot. Because the first pole is three to four magnitudes smaller than the other poles and zeros, it will mainly determine the modulation bandwidth, so $H(s)\approx 1/(s/|p_1|+1)$ in the Bode plot. For cubic equations, we have $p_1p_2+p_2p_3+p_1p_3=D/B$, and $p_1p_2p_3=-1/B$, leading to $1/p_1+1/p_2+1/p_3=-1/D$. For p_1 is much smaller than p_2 and p_3, we get $|1/p_1|\approx|D|$. Substituting $|1/p_1|$ with $|D|$ in the expression of H(s), and keeping in mind that D is positive in the whole locking region; one can approximate the frequency response as,

$$H(s) = \frac{1}{sD+1} \tag{44}$$

where D is given by $(\tau_P + 2\tau_2) + \tau_P/(G_0P_0\tau_3)$. The definition of 3-dB bandwidth is defined as $|H(s)|$ at half of its zero value, i.e. $|H(s)|_{f3dB}| = 1/2$ in the case of normalized frequency response. An approximated expression for 3-dB bandwidth is given as,

Received 15 Nov 2011; accepted 1 Dec 2011; published 9 Jan 2012

$$f_{3\mathrm{dB}} \approx \frac{\sqrt{3}}{2\pi D} = \frac{\sqrt{3}}{2\pi\left[(\tau_P + 2\tau_2) + \dfrac{\tau_p}{G_0 P_0 \tau_3}\right]} \tag{45}$$

Combining the D and $f_{3\mathrm{dB}}$, we can easily see that a larger value of τ_p leads to a decreased modulation bandwidth. This can also be seen from the simulated frequency responses of QCLs at 4.6 μm and 9 μm. Due to larger optical loss, e.g. free carrier absorption (proportional to λ^2) and intersubband absorption in the waveguide, the photon lifetime is much shorter for longer emission wavelengths, leading to an increased modulation bandwidth. However, a larger τ_p means a decreased optical loss, leading to a higher optical output. Thus, the tradeoff between the modulation bandwidth and the output optical power has to be taken into account when designing QCLs for high speed modulation applications. Another feature of QCLs is the absence of resonance peak as normally shown in conventional diode lasers. The physics behind it lies in the ultrafast upper state lifetime compared with the photon lifetime, making QCLs an overdamped system, showing no resonance peak in the frequency modulation response.

3.2 Injection locking modulations

To further enhance the modulation bandwidth of QCLs in the mid-IR regime, we can employ injection locking scheme for QCLs, the theoretical analysis of which is shown in section 2.2. All the additional parameters used in injection locking calculation are listed in Table 4, for QCLs emitting at 4.6 μm and 9 μm, respectively. The rest of the parameters which are common to direct modulated QCLs are shown in Tables 1. Though the linewidth enhance factor of QCLs is expected to be zero [22], the experiments showed different values (0.02 ± 0.2 in [23],-0.44 to 2.29 in [24], and −1.8 to −1.7 in [25]). Without loss of generality, we set the linewidth enhancement factor as unity in the calculations.

Table 4. Characteristic parameters of the state-of-the-art QCL at 4.6 μm [17] and 9 μm [18] for injection locking modulation

Parameter	Symbol	Value(4.6 μm/9 μm)
Linewidth enhancement factor	α	1/1
Threshold carrier number difference	N	1.19×10^{6}(#)/1×10^{6}(#)
Threshold current	J_{th}	$7.9\times10^{17}(s^{-1})$/ $1.92\times10^{18}(s^{-1})$
Optical gain coefficient	G	$3\times10^{4}(s^{-1})$/ $1\times10^{5}(s^{-1})$
Coupling rate	f_d	$11.7(ns^{-1})$/$19.5(ns^{-1})$

Under injection locking scheme, four equations are involved in the calculations. This results in a four-order denominator and a two-order numerator in the frequency response. The typical locking maps for both of QCLs at 4.6 μm and 9μm are illustrated in Fig. 2.(a) and (b), respectively, with $J = 4J_{\mathrm{th}}$. In our simulations, the boundaries of phase in the injection locking range are approximately $\cot^{-1}\alpha$ to -π/2, from negative to positive detuning edge. This is derived from rate equations for the field magnitude E and phase difference ϕ, where the noise terms and spontaneous terms are neglected. The calculated locking maps of QCLs are similar to those of diode lasers, where the locking range increases linearly with the increase of the amplitude of the injected optical field, as demonstrated in Ref [26].

#158118 - $15.00 USD Received 15 Nov 2011; accepted 1 Dec 2011; published 9 Jan 2012

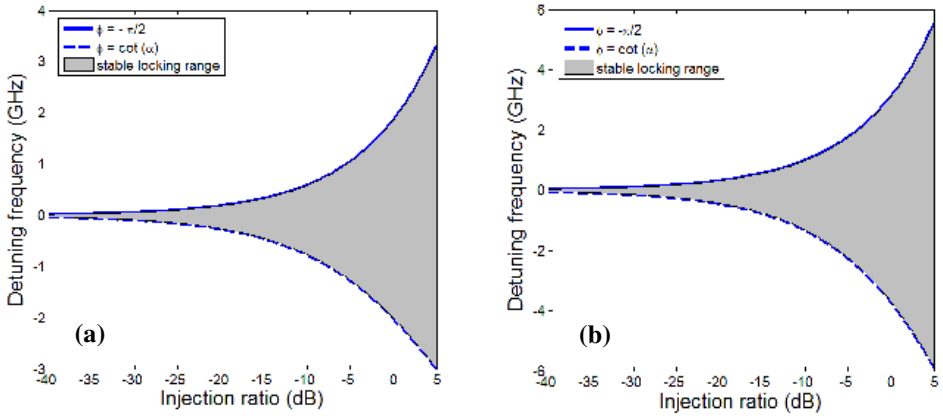

Fig. 2. Locking maps for QCLs emitting at (a) 4.6 μm and (b) 9 μm. The parameters used in the simulations are shown in Tables 1 and 4.

To examine the frequency response of the injection locked QCLs, we calculate the response curves of QCLs at 9 μm with an injection ratio of 5 dB across the locking range and a frequency spacing of 1 GHz. The corresponding waterfall plot is shown in Fig. 3. Table 5 lists the accompanying poles, zeros and 3 dB bandwidth of the responses.

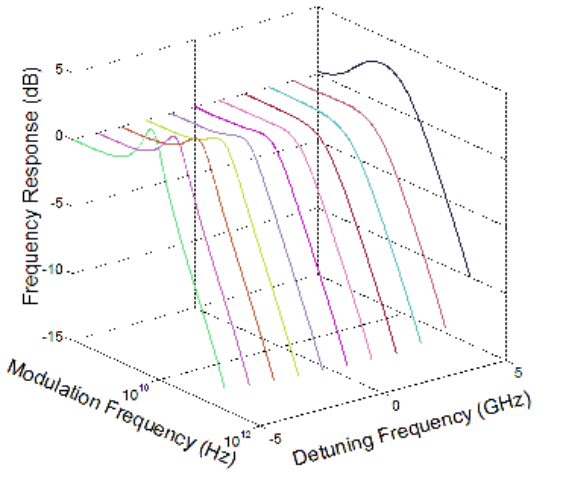

Fig. 3. Normalized frequency response curves versus frequency detuning at a fixed injection ratio R = 5 dB, for the 9 μm QCL.

The frequency response exhibits resonance-like behaviors close to both edges of the locking range (*e.g.* the green and the black curves, respectively, in Fig. 3). However, the reasons behind these two are different. A further explanation can be sought by examining the poles of the frequency response. As illustrated in Table 5, when the frequency comes close to the positive frequency detuning edge (black curve in Fig. 3), two complex conjugate poles appear. In conventional semiconductor lasers, the imaginary part of the complex conjugate poles gives the resonance frequency of the response, while the real part defines the damping term, so that a peak appears in the frequency response. This is also the case for QCLs. At the negative detuning edge (black curve in Fig. 3), because all the poles are real (and negative), the peak in the frequency response has to be analyzed by the Bode Plots. According to the Bode Plots theory, zeros will increase the magnitude of the frequency response from its

#158118 - $15.00 USD
Received 15 Nov 2011; accepted 1 Dec 2011; published 9 Jan 2012

critical frequency and beyond 10 dB per decade, while poles decrease the magnitude at the same rate. For QCLs, the first zero z_1 is smaller than any of the poles, making the peak in the frequency response apparent, even though all the poles are real.

Table 5. Poles, Zeros and 3-dB bandwidth f_{3dB} for the QCL in Fig. 3.

f (GHz)	p_1(GHz)	p_2(GHz)	p_3(GHz)	p_4(GHz)	z_1(GHz)	z_2(GHz)	f_{3dB}(GHz)
–5	–1.6	–9.9	–387.2	–1606.2	–0.7	–895.7	43.6
–4	–2.5	–9.7	–398.7	–1676.0	–2.3	–895.7	18.4
–3	–3.4	–8.8	–400.8	–1690.0	–3.4	–895.7	15.2
–2	–5.1	–6.9	–396.9	–1664.3	–4.2	–895.7	15
–1	–5.8-2.4i	–5.8 + 2.4i	–389.4	–1618.9	–4.7	–895.7	15.6
0	–5.5-3.6i	–5.5 + 3.6i	–379.4	–1563.2	–5.1	–895.7	16.6
1	–5.2-4.5i	–5.2 + 4.5i	–367.6	–1504.4	–5.3	–895.7	18.0
2	–4.7-5.3i	–4.7 + 5.3i	–355.3	–1450.6	–5.4	–895.7	19.2
3	–4.2-5.9i	–4.2 + 5.9i	–342.9	–1401.9	–5.5	–895.7	20.6
4	–3.7-6.5i	–3.7 + 6.5i	–331.2	–1360.6	–5.5	–895.7	21.8
5	–3.0-7.1i	–3.0 + 7.1i	–318.1	–1318.7	–5.5	–895.7	23.4

For conventional semiconductor lasers, increasing slave laser's bias current is an effective way to enhance the bandwidth of the modulation system [12]. Here we calculate the frequency response at a fixed injection ratio of 5 dB, with the injection current varying 1.5x, 2x, 3x, and 4xJ_{th}, respectively, and a frequency detuning 0.1 GHz away from the negative detuning edge, as shown in Fig. 4. The inset is the corresponding pole/zero diagrams. Tables 6 and 7 list the associated poles and zeros of the modulation responses. The increased bandwidth can be attributed to the increased values of poles and zeros of the frequency response, and the much smaller z_1 than any of the poles. Similar effects can also be seen by increasing the injection ratio, for which a much broader modulation bandwidth can be achieved. Our calculation shows that for injection ratio R = 10 dB and frequency detuning of 0.1 GHz away from the edge, over 200 GHz modulation bandwidth can be obtained. However, there is a tradeoff between the injection ratio and the slave laser's injection current, even though both of which can effectively increase the modulation bandwidth. This is because the increased injection current leads to an increased slave laser output power, so that in order to achieve a high injection ratio, a master laser with a higher output power is required, which in some cases is limited in real applications. We noticed that by direct modulating the injection current using an RF source, Pierre et al demonstrated that the cavity resonance frequency of terahertz QCLs can be injection-locked [27]. However, their scheme is different to ours in that the injection signal in our case is the optical signal from the master laser.

It is also noted that there is no unstable locking range in QCLs based on the above rate equation analysis, compared to other types of semiconductor lasers. Mathematically, the stable locking condition is satisfied when the eigenvalues of the frequency response function's denominators are located at the left half of the complex s-plane. In the entire locking region of QCLs, we find that the roots of the denominator are always negative, making the whole locking region a stable locking system. One of the experimental evidence is that the injected light induced pulsation effect [19], which is a unique sign of the unstable locking condition in diode lasers [28] caused by the reduced damping and the strong correlation between the phase and intensity of photons, has not been observed in QCLs. The reasons are as follows: first, there is no relaxation oscillation in QCLs which has been experimentally verified, owing to the picosecond carrier lifetime of the laser states [15]. It is equivalent to say that the damping for the relaxation oscillation is so high such that the carrier numbers and photons come to a steady state in a much shorter time than those in conventional diode lasers. Second, using the phasor diagram and small signal analysis (here we express the small change of N, P, and ϕ as δN, δP and $\delta\phi$), Henry pointed out [28] that the increase of δP

#158118 - $15.00 USD Received 15 Nov 2011; accepted 1 Dec 2011; published 9 Jan 2012

causes an increased $\delta\phi$ in relaxation oscillations. On the other hand, at the negative detuning edge, the increase of $\delta\phi$ causes an enhanced mismatch of E_0 and E_1, leading to a larger cavity intensity change, *i.e.* larger δP. This forms a positive feedback between $\delta\phi$ and δP, which is enhanced as the relaxation oscillations increase. However, there is no relaxation oscillation in QCLs, thus the interaction between $\delta\phi$ and δP is reduced. Therefore the large damping effect and the reduced interactions between ϕ and P, make the unstable locking range in QCLs disappear, as shown in Fig. 2.

Table 6. Poles, zeros, and f_{3dB} for the QCL in Fig. 4 (a)

I_0	p_1(GHz)	p_2(GHz)	p_3(GHz)	p_4(GHz)	z_1(GHz)	z_2(GHz)	f_{3dB}(GHz)
1.5 I_{th}	–0.94	–3.8	–182.5	–845.0	–0.25	–522.2	27.6
2 I_{th}	–1.0	–4.1	–215.1	–1038.2	–0.27	–522.2	30.0
3 I_{th}	–1.1	–4.3	–247.4	–1442.1	–0.29	–522.2	31.8
4 I_{th}	–1.1	–4.4	–263.1	–1857.5	–0.29	–522.2	32.6

Table 7. Poles, zeros, and f_{3dB} for Fig. 4 (b)

I_0	p_1(GHz)	p_2(GHz)	p_3(GHz)	p_4(GHz)	z_1(GHz)	z_2(GHz)	f_{3dB}(GHz)
1.5 I_{th}	–1.5	–9.9	–385.1	–1594.2	–0.50	–895.7	59.2
2 I_{th}	–1.6	–11.3	–434.2	–1971.5	–0.54	–895.7	65.2
3 I_{th}	–1.6	–12.5	–482.0	–2753.1	–0.57	–895.7	69.6
4 I_{th}	–1.6	–13.0	–505.1	–3552.0	–0.58	–895.7	71.4

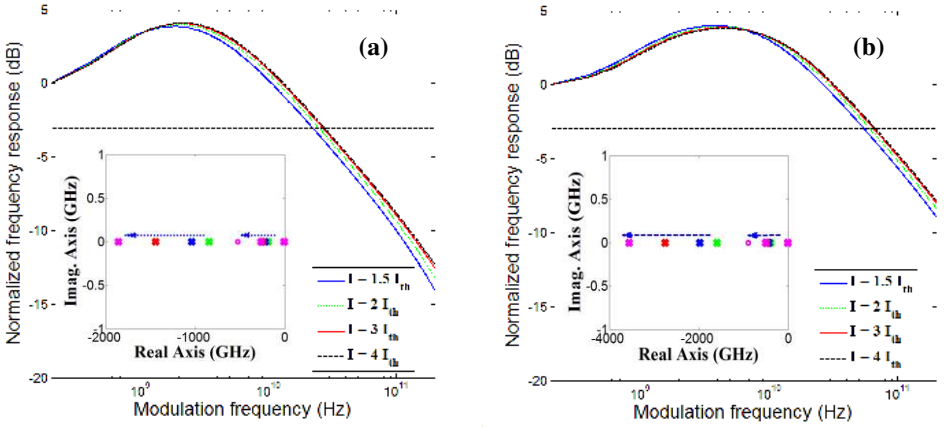

Fig. 4. Normalized modulation response of mid-infrared QCLs under injection locking scheme. (a) QCLs emitting at 4.6 μm. (b) QCLs emitting at 9 μm. The inset show the corresponding poles (x) and zeros (●), with the arrow indicating direction of increasing the injection current of the slave laser. The 3 dB bandwidth is indicated by the dashed line.

4. Conclusions

Theoretical investigation of injection-locked QCLs at wavelengths of 4.6 μm and 9 μm are carried out in the paper. By using a three-level rate equations model, we find that the maximum modulation bandwidths of round 7 GHz for QCLs at 4.6 μm and 20 GHz for QCLs at 9 μm were obtained. It is shown that by applying the injection locking scheme, the modulation bandwidths can be increased by around three times under a 5 dB injection ratio, compared to the direct modulation scheme. The frequency modulation responses were analyzed using the Bode diagram, based on which it shows that increasing the injection ratio and the injected current of the slave laser are effective ways to enhance the modulation

#158118 - $15.00 USD
Received 15 Nov 2011; accepted 1 Dec 2011; published 9 Jan 2012

bandwidth of the master QCLs. With a 10 dB injection ratio, more than 200 GHz modulation bandwidth can be obtained for QCLs at 9 μm. Unlike conventional semiconductor lasers, no unstable locking ranges appear in the locking map, which we attribute to the ultra-short lifetime of the upper laser state of QCLs, due to the nature of intersubband transitions.

#158118 - $15.00 USD
Received 15 Nov 2011; accepted 1 Dec 2011; published 9 Jan 2012